Geophysical Research Letters

RESEARCH LETTER
10.1029/2018GL078961

Special Section:
Initial results of the ERG(Arase) project and multi-point observations in geospace

Drift-Bounce Resonance Between Pc5 Pulsations and Ions at Multiple Energies in the Nightside Magnetosphere: Arase and MMS Observations

S. Oimatsu[1], M. Nosé[1], M. Teramoto[2], K. Yamamoto[1], A. Matsuoka[3], S. Kasahara[4], S. Yokota[5], K. Keika[4], G. Le[6], R. Nomura[7], A. Fujimoto[8], D. Sormakov[9], O. Troshichev[9], Y.-M. Tanaka[10], M. Shinohara[11], I. Shinohara[3], Y. Miyoshi[2], J. A. Slavin[12], R. E. Ergun[13], and P.-A. Lindqvist[14]

[1]Graduate School of Science, Kyoto University, Kyoto, Japan, [2]Institute for Space-Earth Environmental Research, Nagoya University, Nagoya, Japan, [3]Institute of Space and Astronautical Science, Japan Aerospace Exploration Agency, Tokyo, Japan, [4]Graduate School of Science, The University of Tokyo, Tokyo, Japan, [5]Graduate School of Science, Osaka University, Suita, Japan, [6]Heliophysics Science Division, NASA Goddard Space Flight Center, Greenbelt, MD, USA, [7]Environmental Test Technology Unit, Japan Aerospace Exploration Agency, Tokyo, Japan, [8]International Center for Space Weather Science and Education, Kyusyu University, Fukuoka, Japan, [9]Arctic and Antarctic Research Institute, St. Petersburg, Russia, [10]National Institute of Polar Research, Tokyo, Japan, [11]National Institute of Technology, Kagoshima College, Kagoshima, Japan, [12]Department of Climate and Space Sciences and Engineering, University of Michigan, Ann Arbor, MI, USA, [13]Department of Astrophysical and Planetary Sciences, University of Colorado, Denver, CO, USA, [14]Royal Institute of Technology, Stockholm, Sweden

Key Points:
- A large-amplitude Pc5 wave is observed by Arase and MMS1 in the postmidnight region at $L > 5.4$ during the storm recovery phase
- We estimate the *m*-number of the Pc5 wave to be −8 to −15 by using two independent methods with satellites and ground observations
- We simultaneously observe the drift resonance for H^+ and O^+ ions at ≥ 56.3 keV and bounce resonance for O^+ ions at ≤ 18.6 keV

Correspondence to:
S. Oimatsu,
oimatsu@kugi.kyoto-u.ac.jp

Citation:
Oimatsu, S., Nosé, M., Teramoto, M., Yamamoto, K., Matsuoka, A., Kasahara, S., et al. (2018). Drift-bounce resonance between Pc5 pulsations and ions at multiple energies in the nightside magnetosphere: Arase and MMS observations. *Geophysical Research Letters*, *45*, 7277–7286. https://doi.org/10.1029/2018GL078961

Received 1 JUN 2018
Accepted 11 JUL 2018
Accepted article online 17 JUL 2018
Published online 3 AUG 2018

Abstract A Pc5 wave is observed by the Exploration of energization and Radiation in Geospace Arase satellite in the inner magnetosphere (*L* ~5.4–6.1) near postmidnight (*L*-magnetic local time ~1.8–2.5 hr) during the storm recovery phase on 27 March 2017. Its azimuthal wave number (*m*-number) is estimated using two independent methods with satellites and ground observations to be −8 to −15. The direct measurement of the *m*-number enables us to calculate the resonance energy. The flux oscillations of H^+ and O^+ ions at ≥ 56.3 keV are caused by drift resonance and those of O^+ ions at ≤ 18.6 keV by bounce resonance. Resonances of O^+ ions at multiple energies are simultaneously observed for the first time. The enhancement of the O^+/H^+ flux ratio at ≤ 18.6 keV indicates selective acceleration of O^+ ions through bounce resonance.

Plain Language Summary Geomagnetic pulsations are magnetic fluctuations excited by solar wind or plasma instabilities in the magnetosphere. Pc5 waves are continuous geomagnetic pulsations with a period of 150–600 s. A Pc5 wave was observed in the inner magnetosphere during a magnetic storm on 27 March 2017. It propagated westward with a wave number of 8 to 15 and resonated with charged particles, resulting in oscillations of the H^+ and O^+ ion fluxes at ≥ 56.3 keV and the O^+ ion fluxes at ≤ 18.6 keV. Resonances of O^+ ions at multiple energies are simultaneously observed for the first time. At the same time, the O^+/H^+ flux ratio at ≤ 18.6 keV enhanced corresponding to the O^+ ion flux oscillations, which indicates selective acceleration of O^+ ions through resonances.

1. Introduction

Dynamics of O^+ ions in the inner magnetosphere plays an important role for the ring current development and decay. Researchers have suggested that O^+ ions can be accelerated or decelerated through a wave-particle interaction with ultralow frequency (ULF) waves called drift-bounce resonance (e.g., Keika et al., 2013; Li et al., 1993; Yang, Zong, Fu, Li, et al., 2011). The drift-bounce resonance condition is expressed as

$$\omega - m\omega_d = N\omega_b, \tag{1}$$

where ω is the wave angular frequency, ω_d is the particle bounce-averaged drift angular frequency, ω_b is the particle bounce angular frequency, and N is an integer (Southwood et al., 1969). The drift-bounce resonance condition can be satisfied with odd mode waves when $N = 2k$ (where k is an integer), while it can be satisfied with even mode waves when $N = 2k + 1$ (Southwood & Kivelson, 1982). Particles are accelerated or decelerated by oscillating wave electric field in the azimuthal direction of poloidal ULF waves (e.g., Elkington et al., 2003).

Azimuthal wave number (*m*-number) of ULF waves is an important parameter for the drift-bounce resonance because the resonance mode and energy are strongly dependent on it. ULF waves excited by internal instabilities tend to have a dominant magnetic oscillation in the radial direction and large *m*-number ($|m| > \sim 50$), while ULF waves excited by external sources tend to have a dominant magnetic oscillation in the azimuthal direction and small *m*-number ($|m| < \sim 20$). To estimate the *m*-number, several methods have been proposed: phase delay method using multiple satellites (e.g., Le et al., 2017; Takahashi et al., 1985, 2018) or ground stations (e.g., Baker et al., 2003) and the finite Larmor radius effect method (e.g., Min et al., 2017; Takahashi et al., 2018).

To our knowledge, in these two decades, there have been only six observational studies about the drift-bounce resonance of O^+ ions at <40 keV in which data obtained by Composition and Distribution Function (CODIF) analyzer instrument onboard Cluster satellite were used (Ren et al., 2016, 2017; Yang et al., 2010; Yang, Zong, Fu, Li, et al., 2011; Yang, Zong, Fu, Takahashi, et al., 2011; Zong et al., 2012). Acceleration or deceleration of O^+ ions by the drift-bounce resonance on the dayside has been reported (Yang, Zong, Fu, Li, et al., 2011; Zong et al., 2012). Ren et al. (2017) statistically analyzed the O^+ drift-bounce resonance occurrence and found that most of the events occurred on the dayside and few events in the midnight to dawn region. In addition, most of these previous studies did not determine the *m*-number from direct observations. To clarify the influence of the drift-bounce resonance on the ring current, we need to examine whether the drift-bounce resonance can occur on the nightside and accelerate or decelerate O^+ ions based on the direct measurement of the *m*-number.

In this study, we conduct an event analysis of a Pc5 wave and energetic particle flux oscillations in the nightside inner magnetosphere during the storm recovery phase on 27 March 2017, by using Exploration of energization and Radiation in Geospace Arase and Magnetospheric Multiscale 1 (MMS1) satellites data as well as ground magnetometer data. We directly estimate the *m*-number of the Pc5 wave using two methods: satellite and ground observations. Based on the estimated *m*-number, we examine if the ion flux oscillations are caused by the drift-bounce resonance. Finally, we discuss the selective acceleration of O^+ ions at the resonance energy. The following are considered to be new and significant findings of the present study: (1) we first find the drift-bounce resonance of O^+ ions in the nightside inner magnetosphere at multiple energies that predominantly contribute to the ring current, and (2) such analysis was enabled by the simultaneous observations by the recently launched Arase and the MMS1 satellites.

2. Data Set

The Arase satellite was launched on 20 December 2016 into a highly elliptical orbit with an inclination of ~31°, an apogee of ~6 R_E, and a perigee altitude of ~460 km (Miyoshi et al., 2018). Its spin period is ~8 s, and the spin axis is approximately pointing to the Sun.

Magnetic field data are obtained by the triaxial fluxgate magnetometer for the Magnetic Field Experiment (Matsuoka et al., 2018) onboard Arase with a sampling rate of 256 Hz. We used the spin-averaged (~8 s) data.

Medium-energy particle experiments—ion mass analyzer (MEP-i) instrument (Yokota et al., 2017) carried by Arase can distinguish the following ion species: H^+, He^+, He^{2+}, O^+, O^{2+}, and $O_2{}^+$. MEP-i has 16 azimuthal channels, each of which has a 22.5° field of view to cover 360° field of view. The vector normal to the plane of the azimuthal channels is perpendicular to the spin axis. One spin is divided into 16 sectors. There are 16 energy channels covering ~10 to ~180 keV/q, corresponding to the sweeping voltage of ±5 kV at a maximum. However, the sweeping voltage had been set to ±3 kV during the early phase of data acquisition until 21 April 2017, and the observed energy range is 5.1–109.6 keV/q in the present event. There are three observational modes: normal mode, time-of-flight mode, and solid-state detector mode. We used the two spin-averaged (~16 s) flux data of the normal mode, which yields 16 (azimuthal sectors) × 16 (spin sectors) data in one spin.

Medium-energy particle experiments—electron analyzer (MEP-e) instrument (Kasahara et al., 2018) onboard Arase detects electrons (e^-) with 16 energy channels covering 7.0–87.5 keV.

Magnetic field and electric field data are also obtained by MMS. MMS mission consists of four identical spacecraft in tetrahedral formation, and spacecraft were launched in March 2015 into high inclination orbit with an apogee and a perigee of 12 and 1.2 R_E, respectively (Burch et al., 2016). The fluxgate magnetometer measures

the magnetic fields (Russell et al., 2016), and the electric field double probes measure the electric fields (Ergun et al., 2016; Lindqvist et al., 2016). We surveyed the magnetic field and electric field data with a 0.125-s resolution.

Additional data set used in this study comes from ground geomagnetic observations at Tixie (TIK, 62.35° geomagnetic latitude, 194.71° geomagnetic longitude) and Pebek (PBK, 64.31° geomagnetic latitude, 225.14° geomagnetic longitude). These geomagnetic field data have a 1-s sampling rate.

3. Observations of the 27 March 2017 Event

3.1. Pc5 Wave Observations

Figures 1a and 1b show the spacecraft orbits during 18:20–19:10 universal time (UT) on 27 March 2017 in the L-magnetic local time (MLT) plane and in the $\sqrt{X_{SM}^2 + Y_{SM}^2} - Z_{SM}$ plane, where SM denotes the solar magnetic coordinates. The Arase spacecraft is located in the postmidnight region at L = 5.4–6.1 and magnetic latitude (MLAT) = −32° to −25° during the recovery phase of a geomagnetic storm with the minimum Dst of −74 nT (not shown here). MMS1 is located near Arase in MLT (Figure 1a) and gradually moving to higher latitude (Figure 1b). The separations between Arase and MMS1 in L, MLT, and MLAT are ΔL ~2.0, ΔMLT ~0.9 hr, and ΔMLAT ~9°, respectively. In this time interval, only the MMS1 satellite is located close to Arase, while the other MMS satellites are far from the Arase and MMS1 satellites. Figure 1c illustrates the footprints of Arase and MMS1 calculated with the Tsyganenko 89 model (Tsyganenko, 1989) at 18:20–19:10 UT and location of the ground stations (PBK and TIK) in geographic coordinates.

Figures 1d–1f illustrate the magnetic field observed by Arase at 18:20–19:10 UT in the mean field aligned coordinates, in which 10-min moving averages are subtracted, and the radial component is perpendicular to the International Geomagnetic Reference Field-12 (Thébault et al., 2015) model field and radially outward (B_r), and the azimuthal component (B_a) is perpendicular to both the parallel (B_p) and radial components to complete the right-handed orthogonal system. A Pc5 wave has large amplitudes in both B_r and B_a, and the peak-to-peak amplitude of B_a (~30 nT) is larger than that of B_r (~10 nT). This is the evidence of an external source and a mode coupling between poloidal and toroidal modes (e.g., Takahashi et al., 2018). Figure 1g illustrates the 10-s averaged B_r and E_a observed by MMS1. We find that Pc5 wave oscillations appear in both B_r and E_a, and the peak-to-peak amplitude of B_a (~12 nT, not shown) is also larger than that of B_r (~8 nT). In addition, E_a leads B_r by ~90° at 18:30–19:05 UT. This is the characteristic of odd mode standing oscillations in the Southern Hemisphere (e.g., Dai et al., 2013). Since the wave period of the Pc5 wave is quite long (~450 s), this Pc5 wave is likely a fundamental standing wave. Fundamental mode waves are easily detected in the off-equatorial regions, which is consistent with both Arase and MMS1 observations that the Pc5 waves are clearly observed far from the equatorial plane.

Figure 1h shows the Y (east-west) component of the ground magnetic field at TIK and PBK from which 10-min moving averages are subtracted. These two stations are chosen because they are located close to the satellite footprints as shown in Figure 1c. A Pc5 wave with a period similar to that observed by Arase is detected at both stations. Figure 2a illustrates the power spectra of B_r observed by Arase, B_r, and E_a observed by MMS1 and Y component of the magnetic field at TIK and PBK during 18:30–19:10 UT. We find spectral peaks at 2–2.5 mHz in all power spectra, which indicates that the Pc5 waves observed by Arase and MMS1, and the ground magnetometers at TIK and PBK are identical.

3.2. Particle Flux Oscillations Observed by MEP

We investigate the particle fluxes measured by MEP-i and MEP-e. Figures 1i–1k are the 60-s averaged omnidirectional residual fluxes $((J - J_0)/J_0)$, where J is the particle flux and J_0 is the 10-min moving average of H^+ and O^+ ions and of electrons. Figure 1i shows that H^+ fluxes in wide energy ranges oscillate with the Pc5 wave period, and their oscillation amplitudes are large at $\geq$ 56.3 keV during 18:30–19:10 UT. Figure 1j shows that the O^+ ion fluxes are also clearly modulated at 18:30–19:10 UT with the same period of the Pc5 wave. The oscillation amplitudes are larger at $\geq$ 56.3 and $\leq$ 18.6 keV. We can find negative energy dispersions (e.g., Southwood & Kivelson, 1981) for both H^+ at $\geq$ 56.3 keV and O^+ ion fluxes at $\geq$ 56.3 and $\leq$ 18.6 keV in Figures 1i and 1j, respectively. Despite the large electron flux oscillations at

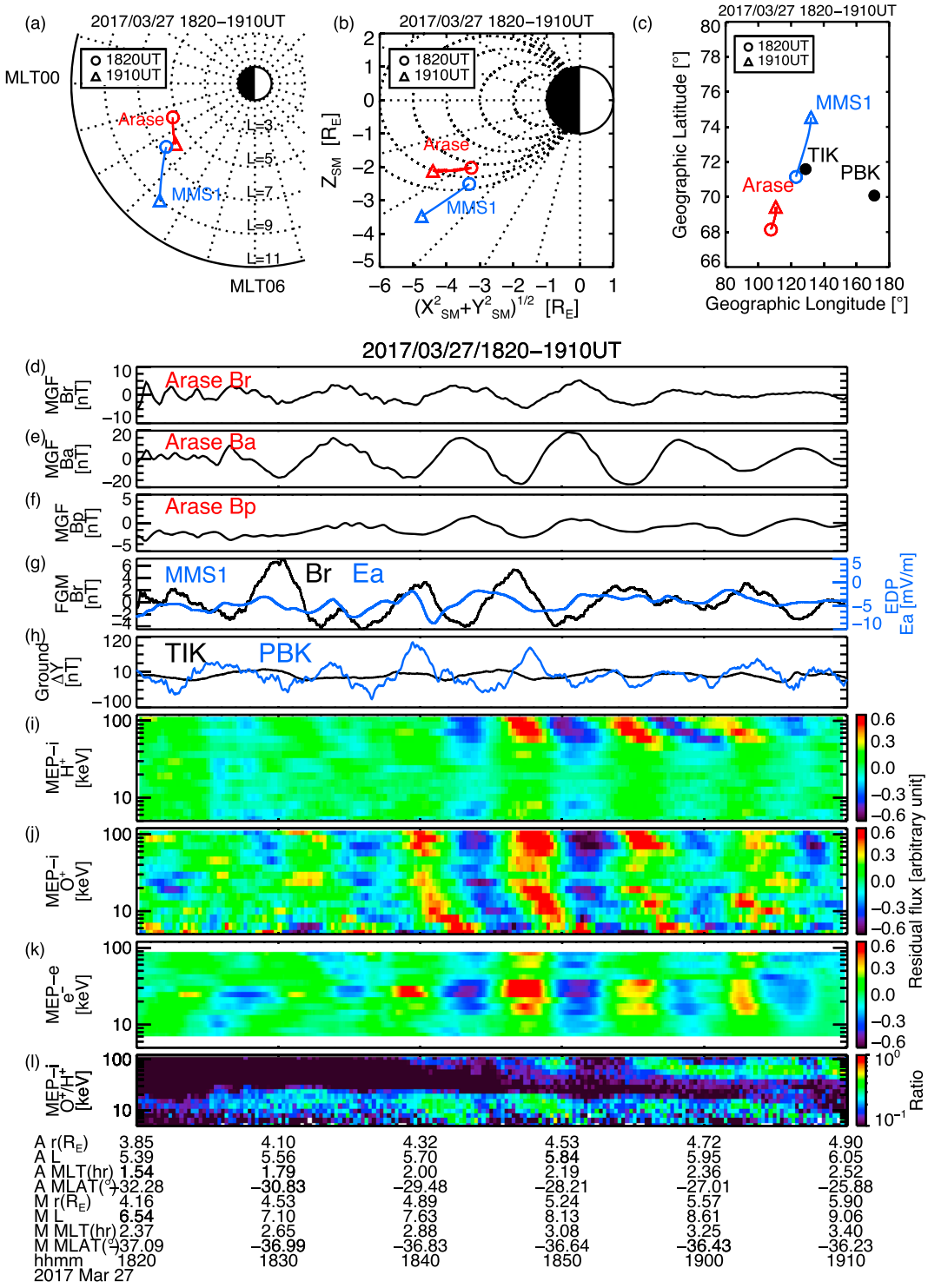

Figure 1. Satellite orbits, satellite data, and ground station data for 18:20–19:10 UT on 27 March 2017. First letters A and M of orbit information denote Arase and MMS1, respectively. (a) Arase and MMS1 satellite orbits in the *L*-MLT plane. (b) Arase and MMS1 orbits in the $\sqrt{X^2_{SM}+Y^2_{SM}}-Z_{SM}$ plane of SM coordinates. (c) Satellite footprints and the location of the ground magnetic stations at Tixie (TIK) and Pebek (PBK) in geographic coordinates. (d, e, f) Magnetic fields in radial (B_r), azimuthal (B_a), and parallel components (B_p) observed by MGF. (g) Magnetic field in the radial component (black) and electric field in the azimuthal component (E_a, blue) observed by MMS1. (h) Ground magnetic field in the Y (east-west) component at TIK (black) and PBK (blue). (i, j, k) The 60-s averaged residual fluxes of H^+ and O^+ ions detected by MEP-i and 60-s averaged residual flux of electrons detected by MEP-e. (l) O^+/H^+ ratio of the omnidirectional fluxes.

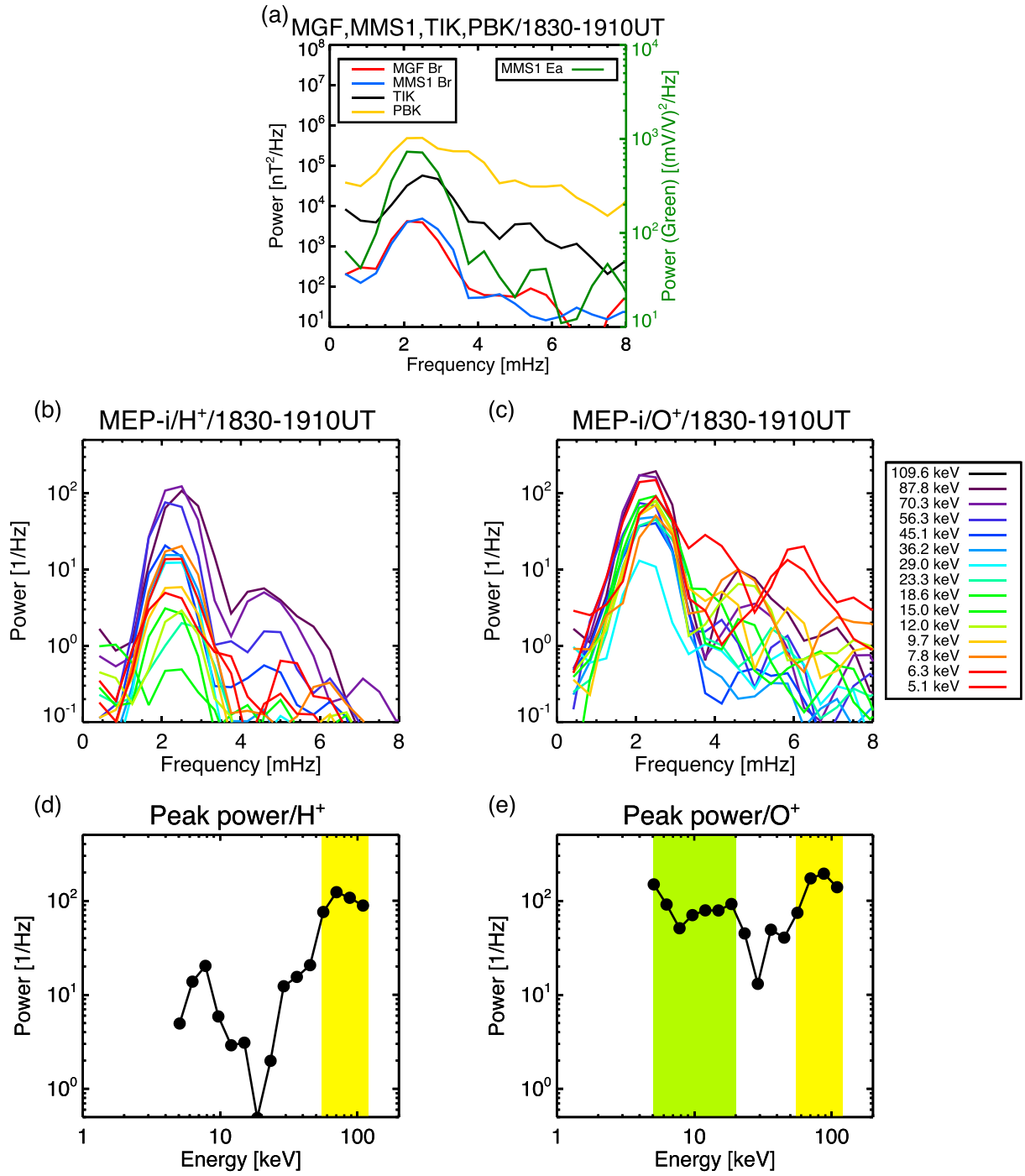

Figure 2. (a) Power spectra of the magnetic field in the radial component observed by MGF and MMS1, the magnetic field in the Y component observed at TIK and PBK, and the electric field in the azimuthal component observed by MMS1 at 18:30–19:10 UT. (b, c) Power spectra of the residual fluxes of H^+ and O^+ ions detected by medium-energy particle experiments—ion mass analyzer at 18:30–19:10 UT. Colors delineate different energies as indicated in the legend. (d, e) Spectral peak power of H^+ and O^+ ion fluxes at ~2–3 mHz as a function of energies.

14.3–35.0 keV, the energy dispersion signature cannot be seen in Figure 1k. We calculate the omnidirectional flux ratio of O^+/H^+ (Figure 1l), which exhibit a distinct structure in the O^+/H^+ flux ratio. The ratio is ~0.1 until 18:25 UT, and then it reaches the maximum of ~0.4 at $\leq$ 23.3 and $\geq$ 45.1 keV during 18:40–19:10 UT, corresponding to the O^+ ion flux oscillations.

Figures 2b and 2c illustrate the power spectra of the residual fluxes $((J - J_0)/J_0)$ of H^+ and O^+ ions at different energies. Clear spectral peaks can be seen in wide energy ranges for both H^+ and O^+ ions at 2–2.5 mHz, which is similar to the Pc5 wave frequency. The spectral peaks of O^+ ions are larger than those of H^+. In Figures 2d and 2e, we plot power spectral peaks for H^+ and O^+ ions near 2–2.5 mHz for different energies. The peak power of H^+ at $\geq$ 56.3 keV is more than ~3 times larger than that at lower energies. It also should be noted that we can find a small peak at ~7 keV (Figure 2d), though the width of the peak is too narrow without plateau structure like that at high energy, indicating that the H^+ flux oscillations mainly occur at higher energies. Figure 2e shows two energy bands with large peak power for O^+ ions at $\geq$ 56.3 and $\leq$ 18.6 keV, while there is a dip of the peak power of O^+ ions at 23.3–45.1 keV. This structure of the peak power is similar to that of O^+/H^+ in Figure 1l, suggesting a relation between O^+ ion oscillations and the O^+/H^+ structure. The power enhancement of H^+ and O^+ ions may extend up to $\geq$ 109.6 keV, which cannot be detected with the MEP-i.

4. Discussion

The value of the *m*-number generally reflects the energy source of Pc5 waves: external solar wind for a small *m*-number or internal plasma instability for a large *m*-number. Also, the drift-bounce resonance mode and the resonance energy strongly depend on the *m*-number. In this section, we estimate the value of the *m*-number and discuss the energy source and the resonance characteristics.

4.1. Estimation of *m*-Number of the Pc5 Wave

The Pc5 wave is observed by Arase, MMS1, and ground stations at TIK and PBK. We examine the *m*-number by two methods.

First, we estimate the *m*-number using Arase and MMS1 data. Figure 1a shows that both satellites are close to each other in MLT but not close in *L*. To calculate the *m*-number, we assume that the wave structure is uniform in *L*. We can estimate the *m*-number from a phase delay of the Pc5 waves observed by two satellites that are azimuthally separated; that is, $m = \Delta\theta/\Delta\varphi$, where $\Delta\theta$ is the phase difference, and $\Delta\varphi$ is the azimuthal separation between satellites. Figures 1d and 1g show a clear time lag in B_r. We determine a time lag that provides the maximum value of the cross-correlation coefficient between B_r observed by Arase and MMS1. Cross-correlation analysis shows that the time delay is 240 s at 18:30–19:10 UT. Since Figure 2a shows the wave period of ~ 450 s, we obtain $\Delta\theta \sim -192°$, where the negative sign means westward propagation. The $\Delta\varphi$ between Arase and MMS1 is ~13° at 18:30–19:10 UT. Thus, these values of $\Delta\varphi$ and $\Delta\theta$ give $m \sim -15$.

Second, we estimate the *m*-number using ground magnetometer data at TIK and PBK with the same method as first estimation. The cross-correlation analysis at 18:30–19:10 UT gives 305-s time delay between TIK and PBK, which corresponds to $\Delta\theta \sim -244°$, and $\Delta\varphi = 30.4°$ in the geomagnetic coordinate. Then, *m*-number is estimated to be $m \sim -8$.

From the two independent methods, we obtain the similar values of $m \sim -8$ to -15. (Although there is a possibility that the phase difference includes a $2n\pi$ ambiguity, the cross-correlation coefficients become maximum when $n = 0$.) These values are consistent with the fact that the Pc5 wave is observed on the ground with a less ionospheric screening effect. According to Hughes and Southwood (1976), the wave amplitude of $|m| = 10$ on the ground is ~86% that of $m = 0$. The westward propagation in the morning sector is also consistent with the result of previous studies (e.g., Baker et al., 2003).

4.2. Energy Source of the Pc5 Wave

Pc5 waves are mainly excited on the dayside magnetosphere by the Kelvin-Helmholtz instability due to high solar wind velocity, solar wind dynamic pressure variation, and ion foreshock (e.g., Takahashi et al., 2016; Ukhorskiy et al., 2009). Past studies on ULF wave distributions showed that Pc5 waves can occur in the dawn to the postmidnight region (e.g., Anderson et al., 1990; Liu et al., 2009; Nosé et al., 1995). The Pc5 wave in the present study has quite large amplitude in the azimuthal component of the magnetic field on the nightside (Figure 1e) when the solar wind velocity is high (~600–650 km/s) according to the OMNI database. Pc5 waves excited by solar wind tend to have small *m*-number, which is consistent with the above result ($m \sim -8$ to -15). Thus, we suggest that this Pc5 wave is excited by solar wind, not by internal plasma instabilities.

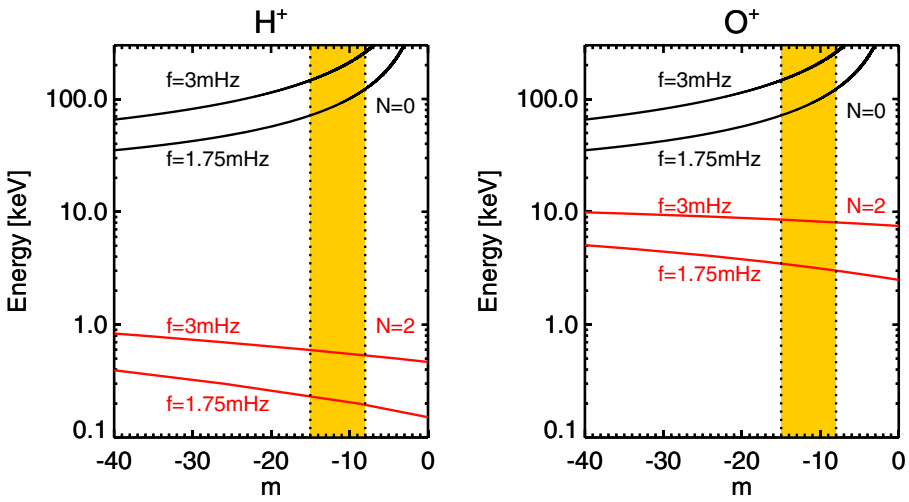

Figure 3. Resonance energies of H^+ and O^+ ions with fundamental mode ($N = 0, 2$) waves as a function of m, when a dipole magnetic field is assumed. We use frequencies of 1.75 and 3 mHz, $L = 5.8$, and a local pitch angle of 90° to calculate the energy.

4.3. Examination of the Flux Oscillations

Flux oscillations associated with ULF waves are often observed in the magnetosphere. Betatron acceleration, drift-bounce resonant interaction, and radial convection of particles are proposed as the reason of the flux oscillations (e.g., Korotova et al., 2015; Southwood & Kivelson, 1981; Takahashi et al., 1985). Direct measurements of the m-number from the satellite and ground observations enable us to calculate the resonance energy based on equation (1).

The approximation of ω_b and ω_d in a dipole magnetic field are given by $\omega_b = \frac{\pi\sqrt{2W/m_i}}{2LR_E T(\sin\alpha_E)}$ and $\omega_d = -\frac{6WLP(\sin\alpha_E)}{qB_E R_E{}^2} + \frac{2\psi_0 L^3 \sin\varphi}{B_E R_E{}^2} + \Omega_E$, where m_i is the ion mass, R_E is the Earth's radius, α_E is the pitch angle at the geomagnetic equator, B_E is the equatorial magnetic field at the surface of the Earth, q is the electric charge, φ is the azimuthal angle which is positive eastward with 0° at midnight, Ω_E is the angular frequency of the corotation of the Earth, and ψ_0 is the electric potential of the convection electric field. We adopt B_E = 30,000 nT and the following formulae: $T(\sin\alpha_E) = 1.351 - 0.925\sin\alpha_E + 0.558\sin^2\alpha_E - 0.248\sin^3\alpha_E$ and $P(\sin\alpha_E) = 0.340 + 0.226\sin\alpha_E - 0.154\sin^2\alpha_E + 0.088\sin^3\alpha_E$ (Hamlin et al., 1961; Oimatsu et al., 2018; Yang, Zong, Fu, Li, et al., 2011). We use the Volland-Stern model electric potential as ψ_0 (Maynard & Chen, 1975; Stern, 1975; Volland, 1973). Figure 3 shows the theoretical drift-bounce resonance energy with fundamental mode wave ($N = 0$ and 2) as a function of the m-number in a dipole magnetic field for H^+ and O^+ ions. Particles with equatorial pitch angle of 90° most effectively resonate with fundamental mode waves. In general, ULF waves are not monochromatic, and wave frequency and m-number have a finite bandwidth (e.g., Korotova et al., 2015; Takahashi et al., 1990). We use wave frequencies of 1.75 and 3 mHz, $L = 5.8$, and a local pitch angle of 90° to calculate the resonance energy. The vertical dashed lines denote $m = -8$ and -15, which are estimated from the satellite and ground observations, respectively. There are two solutions: $\omega \sim m\omega_d$ ($N = 0$, drift resonance) and $\omega \sim 2\omega_b$ ($N = 2$, bounce resonance). For the finite bandwidths of m-number and wave frequency, the drift resonance energies of H^+ and O^+ ions are estimated to be ~70–200 keV for both ion species, and the bounce resonance energies are estimated to be ~0.2–0.6 keV for H^+ and ~3–9 keV for O^+ ions. These results of the theoretical resonance energy are generally consistent with the observational facts of large power spectral peaks for both H^+ and O^+ ions at $\geq$ 56.3 keV (drift resonance) and for O^+ ions at $\leq$ 18.6 keV (bounce resonance) in Figures 2d and 2e, respectively.

Drift-bounce resonance theory predicts a 180° phase shift over the resonance energy (e.g., Southwood & Kivelson, 1981; Takahashi et al., 1990). Figures 1i and 1j show the dispersive flux peaks for H^+ at $\geq$ 56.3 keV and for O^+ ions at $\geq$ 56.3 keV and $\leq$ 18.6 keV, which are similar to the past observational results (e.g., Ren et al., 2016). This implies the drift-bounce resonance for H^+ and O^+ ions because of the measurable phase shifts

over the energy channels. In this study, the drift resonance and bounce resonance for O^+ ions are simultaneously observed for the first time. Previous studies found O^+ drift-bounce resonance at $\leq$ 40 keV because of the instrument limitation of the energy coverage. The wide energy coverage of MEP-i enables us to find the resonances at multiple energies. The phase shift of O^+ ion flux at $\leq$ 18.6 keV is much larger than those of H^+ and O^+ ion fluxes at $\geq$ 56.3 keV (Figures 1i and 1j). We suppose that the drift resonance energy, which is estimated to be 70–200 keV from the theoretical calculations, is close to or higher than the upper limit of the energy coverage of MEP-i (109.6 keV), and consequently, the overall phase shifts cannot be detected. Electron fluxes at 14.3–35.0 keV oscillate, but they do not show energy dispersion (Figure 1k), indicating that the electron flux oscillations are not caused by the drift-bounce resonance.

The observed Pc5 wave has a toroidal mode component. If there is a gradient of particle flux distribution in the azimuthal direction, toroidal mode waves can influence the particle fluxes. However, the variation of the particle distribution in the azimuthal direction is expected to be smaller than that in the radial direction. Therefore, the particle fluctuations are mainly generated by poloidal mode waves.

4.4. Implication of Selective Acceleration of O^+ Ions

O^+/H^+ flux ratio becomes high at two energy bands ($\leq$ 23.3 and $\geq$ 45.1 keV) corresponding to the energy ranges of the drift resonance and the bounce resonance of ions during 18:30–19:10 UT in Figure 1l. One may think that this is caused by the spatial effect. However, in such case, the O^+/H^+ ratio is expected to become high in wider energy ranges, unlike what shown by the present results. Hence, we suggest that the enhancement of O^+/H^+ flux ratio in the low-energy band ($\leq$ 23.3 keV) is mainly caused by selective acceleration of O^+ ions due to the bounce resonance at $\leq$ 18.6 keV, because only the bounce resonance of O^+ ions occurs without that of H^+ ions at the same energy. It would be appropriate to consider that the solar wind generates the Pc5 wave and it feeds energy to the O^+ ions through the bounce resonance. Mitani et al. (2018) proposed that the drift-bounce resonance contributes to the selective penetration of O^+ ions into the inner magnetosphere from the plasma sheet during the late main phase to early recovery phase, which is consistent with our scenario. The present study first demonstrates the selective acceleration of O^+ ions due to the bounce resonance in the nightside inner magnetosphere. The enhancement of the O^+/H^+ flux ratio in the high-energy band ($\geq$ 45.1 keV) may be due to the acceleration efficiency of the drift resonance between H^+ and O^+ ions ($\geq$ 56.3 keV). It should be examined in the future how effectively the drift resonance take place for H^+ and O^+ ions, which is expected to depend on the radial and energy gradients of the phase space density of ion species (e.g., Southwood et al., 1969).

5. Conclusions

We first examine the drift-bounce resonance between a fundamental mode Pc5 pulsation and O^+ ions in the nightside inner magnetosphere at L = 5.4–6.1 during a storm recovery phase on 27 March 2017, using data from Arase, MMS1, and ground magnetometers at TIK and PBK. We directly estimate the m-number of the Pc5 wave to be $m \sim -8$ to -15 by two independent methods using satellites and ground observations. The H^+ fluxes show the largest oscillation amplitude at $\geq$ 56.3 keV, and the O^+ ion fluxes also show the largest amplitude at the same energy ($\geq$ 56.3 keV) and at $\leq$ 18.6 keV. The O^+/H^+ flux ratio becomes higher during the ion flux oscillations at $\leq$ 23.3 and $\geq$ 45.1 keV. The theoretical drift resonance energy is ~70–200 keV for both H^+ and O^+ ions, while the theoretical bounce resonance energy is ~3–9 keV for O^+ ions. These theoretical resonance energies are consistent with the results of the Arase/MEP-i observation. The H^+ and O^+ ion oscillations at $\geq$ 56.3 keV are generated through the drift resonance, while the O^+ ion oscillations at $\leq$ 18.6 keV are caused by the bounce resonance. These resonances of O^+ ions at multiple energies are simultaneously observed for the first time. The enhancement of the O^+/H^+ flux ratio at $\leq$ 18.6 keV indicates a selective acceleration of O^+ ions due to the bounce resonance.

Acknowledgments
We thank Dr. K. Takahashi for his valuable comments. We appreciate all people dedicated to the Arase mission. The works of M. T. and Y. M. were partly done at ERG-SC. Science data of the Arase satellite were obtained from the ERG Science Center operated by ISAS/JAXA and ISEE/Nagoya University (http://ergsc.isee.nagoya-u.ac.jp/index.shtml.en). The Arase satellite data will be publicly available via ERG Science Center on a project-agreed schedule. The present study analyzed the MGF L2 v01.01 data, the MEP-i L2 v01_00 data, and the MEP-e L2 v01_00 data. The magnetic field and electric field data observed by FGM and EDP onboard MMS1 are available via MMS science data center at https://lasp.colorado.edu/mms/sdc/public/. Solar wind data were obtained from OMNI database at https://omniweb.gsfc.nasa.gov. The Dst index was provided by the World Data Center for Geomagnetism, Kyoto, and is available at http://wdc.kugi.kyoto-u.ac.jp. This study is supported by Japan Society for the Promotion of Science (JSPS), Grant-in-Aid for Scientific Research (B) (grant 16H04057), Challenging Research (Pioneering) (17K18804), Grant-in-Aid for Specially Promoted Research (16H06286), and Grant-in-Aid for Young Scientists (B) (grant 17K14400). Y. M. is supported by Japan Society for the Promotion of Science (JSPS), Grant-in-Aid for Scientific Research on Innovative Areas (grant 15H05815).

References

Anderson, B. J., Engebretson, M. J., Rounds, S. P., Zanetti, L. J., & Potemra, T. A. (1990). A statistical study of Pc 3–5 pulsations observed by the AMPTE/CCE Magnetic Fields Experiment, 1. Occurrence distributions. *Journal of Geophysical Research*, *95*(A7), 10,495–10,523. https://doi.org/10.1029/JA095iA07p10495

Baker, G., Donovan, E. F., & Jackel, B. J. (2003). A comprehensive survey of auroral latitude Pc5 pulsation characteristics. *Journal of Geophysical Research*, *108*(A10), 1384. https://doi.org/10.1029/2002JA009801

Burch, J. L., Moore, T. E., Torbert, R. B., & Giles, B. L. (2016). Magnetospheric multiscale overview and science objectives. *Space Science Reviews*, *199*(1–4), 5–21. https://doi.org/10.1007/s11214-015-0164-9

Dai, L., Takahashi, K., Wygant, J. R., Chen, L., Bonnell, J., Cattell, C. A., et al. (2013). Excitation of poloidal standing Alfvén waves through drift resonance wave-particle interaction. *Geophysical Research Letters*, *40*, 4127–4132. https://doi.org/10.1002/grl.50800

Elkington, S. R., Hudson, M. K., & Chan, A. A. (2003). Resonant acceleration and diffusion of outer zone electrons in an asymmetric geomagnetic field. *Journal of Geophysical Research*, *108*(A3), 1116. https://doi.org/10.1029/2001JA009202

Ergun, R. E., Tucker, S., Westfall, J., Goodrich, K. A., Malaspina, D. M., Summers, D., et al. (2016). The Axial Double Probe and fields signal processing for the MMS mission. *Space Science Reviews*, *199*(1–4), 167–188. https://doi.org/10.1007/s11214-014-0115-x

Hamlin, D. A., Karplus, R., Vik, R. C., & Watson, K. M. (1961). Mirror and azimuthal drift frequencies for geomagnetically trapped particles. *Journal of Geophysical Research*, *66*(1), 1–4. https://doi.org/10.1029/JZ066i001p00001

Hughes, W. J., & Southwood, D. J. (1976). The screening of micropulsation signals by the atmosphere and ionosphere. *Journal of Geophysical Research*, *81*(19), 3234–3240. https://doi.org/10.1029/JA081i019p03234

Kasahara, S., Yokota, S., Mitani, T., Asamura, K., Hirahara, M., Shibano, Y., & Takashima, T. (2018). Medium-energy particle experiments electron analyzer (MEP-e) for the exploration of energization and radiation in geospace (ERG) mission. *Earth, Planets and Space*, *70*(1), 69. https://doi.org/10.1186/s40623-018-0847-z

Keika, K., Kistler, L. M., & Brandt, P. C. (2013). Energization of O^+ ions in the Earth's inner magnetosphere and the effects on ring current buildup: A review of previous observations and possible mechanisms. *Journal of Geophysical Research: Space Physics*, *118*, 4441–4464. https://doi.org/10.1002/jgra.50371

Korotova, G. I., Sibeck, D. G., Tahakashi, K., Dai, L., Spence, H. E., Kletzing, C. A., et al. (2015). Van Allen Probe observations of drift-bounce resonances with Pc 4 pulsations and wave-particle interactions in the pre-midnight inner magnetosphere. *Annales de Geophysique*, *33*(8), 955–964. https://doi.org/10.5194/angeo-33-955-2015

Le, G., Chi, P. J., Strangeway, R. J., Russell, C. T., Slavin, J. A., Takahashi, K., et al. (2017). Global observations of magnetospheric high-m poloidal waves during the 22 June 2015 magnetic storm. *Geophysical Research Letters*, *44*, 3456–3464. https://doi.org/10.1002/2017GL073048

Li, X., Hudson, M., Chan, A., & Roth, I. (1993). Loss of ring current O^+ ions due to interaction with Pc 5 waves. *Journal of Geophysical Research*, *98*(A1), 215–231. https://doi.org/10.1029/92JA01540

Lindqvist, P. A., Olsson, G., Torbert, R. B., King, B., Granoff, M., Rau, D., et al. (2016). The spin-plane double probe electric field instrument for MMS. *Space Science Reviews*, *199*(1–4), 137–165. https://doi.org/10.1007/s11214-014-0116-9

Liu, W., Sarris, T. E., Li, X., Elkington, S. R., Ergun, R., Angelopoulos, V., et al. (2009). Electric and magnetic field observations of Pc4 and Pc5 pulsations in the inner magnetosphere: A statistical study. *Journal of Geophysical Research*, *114*, A12206. https://doi.org/10.1029/2009JA014243.

Matsuoka, A., Teramoto, M., Nomura, R., Nosé, M., Fujimoto, A., Tanaka, Y., et al. (2018). The ARASE (ERG) magnetic field investigation. *Earth, Planets and Space*, *70*(1), 43. https://doi.org/10.1186/s40623-018-0800-1

Maynard, N. C., & Chen, A. J. (1975). Isolated cold plasma regions: Observations and their relation to possible production mechanisms. *Journal of Geophysical Research*, *80*(7), 1009–1013. https://doi.org/10.1029/JA080i007p01009

Min, K., Takahashi, K., Ukhorskiy, A. Y., Manweiler, J. W., Spence, H. E., Singer, H. J., et al. (2017). Second harmonic poloidal waves observed by Van Allen Probes in the dusk-midnight sector. *Journal of Geophysical Research: Space Physics*, *122*, 3013–3039. https://doi.org/10.1002/2016JA023770

Mitani, K., Seki, K., Keika, K., Gkioulidou, M., Lanzerotti, L. J., Mitchell, D. G., & Kletzing, C. A. (2018). Radial transport of higher-energy oxygen ions into the deep inner magnetosphere observed by Van Allen Probes. *Geophysical Research Letters*, *45*, 4534–4541. https://doi.org/10.1029/2018GL077500

Miyoshi, Y., Shinohara, I., Takashima, T., Asamura, K., Higashio, N., Mitani, T., et al. (2018). Geospace exploration project ERG. *Earth, Planets and Space*, *70*(1). https://doi.org/10.1186/s40623-018-0862-0

Nosé, M., Iyemori, T., Sugiura, M., & Slavin, J. A. (1995). A strong dawn/dusk asymmetry in Pc5 pulsation occurrence observed by the DE-1 satellite. *Geophysical Research Letters*, *22*(15), 2053–2056. https://doi.org/10.1029/95GL01794

Oimatsu, S., Nosé, M., Takahashi, K., Yamamoto, K., Keika, K., Kletzing, C. A., et al. (2018). Van Allen Probes observations of drift-bounce resonance and energy transfer between energetic ring current protons and poloidal Pc4 wave. *Journal of Geophysical Research: Space Physics*, *123*, 3421–3435. https://doi.org/10.1029/2017JA025087

Ren, J., Zong, Q.-G., Zhou, X.-Z., Rankin, R., & Wang, Y.-F. (2016). Interaction of ULF waves with different ion species: Pitch angle and phase space density implications. *Journal of Geophysical Research: Space Physics*, *121*, 9459–9472. https://doi.org/10.1002/2016JA022995

Ren, J., Zong, Q. G., Zhou, X. Z., Rankin, R., Wang, Y. F., Gu, S. J., & Zhu, Y. F. (2017). Phase relationship between ULF waves and drift-bounce resonant ions: A statistical study. *Journal of Geophysical Research: Space Physics*, *122*, 7087–7096. https://doi.org/10.1002/2016JA023848

Russell, C. T., Anderson, B. J., Baumjohann, W., Bromund, K. R., Dearborn, D., Fischer, D., et al. (2016). The Magnetospheric Multiscale Magnetometers. *Space Science Reviews*, *199*, 189–256. https://doi.org/10.1007/s11214-014-0057-3

Southwood, D. J., Dungey, J. W., & Etherington, R. J. (1969). Bounce resonant interaction between pulsations and trapped particles. *Planetary and Space Science*, *17*(3), 349–361. https://doi.org/10.1016/0032-0633(69)90068-3

Southwood, D. J., & Kivelson, M. G. (1981). Charged particle behavior in low-frequency geomagnetic pulsations 1. Transverse waves. *Journal of Geophysical Research*, *86*(A7), 5643–5655. https://doi.org/10.1029/JA086iA07p05643

Southwood, D. J., & Kivelson, M. G. (1982). Charged particle behavior in low-frequency geomagnetic pulsations, 2. Graphical approach. *Journal of Geophysical Research*, *87*(A3), 1707–1710. https://doi.org/10.1029/JA087iA03p01707

Stern, D. P. (1975). The motion of a proton in the equatorial magnetosphere. *Journal of Geophysical Research*, *80*(4), 595–599. https://doi.org/10.1029/JA080i004p00595

Takahashi, K., Hartinger, M. D., Malaspina, D. M., Smith, C. W., Koga, K., Singer, H. J., et al. (2016). Propagation of ULF waves from the upstream region to the midnight sector of the inner magnetosphere. *Journal of Geophysical Research: Space Physics*, *121*, 8428–8447. https://doi.org/10.1002/2016JA022958

Takahashi, K., Higbie, P. R., & Baker, D. N. (1985). Azimuthal propagation and frequency characteristic of compressional Pc 5 waves observed at geostationary orbit. *Journal of Geophysical Research*, *90*(A2), 1473–1485. https://doi.org/10.1029/JA090iA02p01473

Takahashi, K., McEntire, R. W., Lui, A. T. Y., & Potemra, T. A. (1990). Ion flux oscillations associated with a radially polarized transverse Pc 5 magnetic pulsation. *Journal of Geophysical Research*, *95*(A4), 3717–3731. https://doi.org/10.1029/JA095iA04p03717

Takahashi, K., Oimatsu, S., Nosé, M., Min, K., Claudepierre, S. G., Chan, A., et al. (2018). Van Allen Probes observations of second-harmonic poloidal standing Alfvén waves. *Journal of Geophysical Research: Space Physics*, *123*, 611–637. https://doi.org/10.1002/2017JA024869

Thébault, E., Finlay, C. C., Beggan, C. D., Alken, P., Aubert, J., Barrois, O., et al. (2015). International Geomagnetic Reference Field: The 12th generation. *Earth, Planets and Space*, *67*(1), 79. https://doi.org/10.1186/s40623-015-0228-9

Tsyganenko, N. A. (1989). A magnetospheric magnetic field model with a warped tail current sheet. *Planetary and Space Science*, *37*(1), 5–20. https://doi.org/10.1016/0032-0633(89)90066-4

Ukhorskiy, A. Y., Sitnov, M. I., Takahashi, K., & Anderson, B. J. (2009). Radial transport of radiation belt electrons due to stormtime Pc5 waves. *Annales de Geophysique*, *27*, 2173–2181. https://doi.org/10.5194/angeo-27-2173-2009

Volland, H. (1973). A semiempirical model of large-scale magnetospheric electric fields. *Journal of Geophysical Research*, *78*(1), 171–180. https://doi.org/10.1029/JA078i001p00171

Yang, B., Zong, Q. G., Fu, S. Y., Li, X., Korth, A., Fu, H. S., et al. (2011). The role of ULF waves interacting with oxygen ions at the outer ring current during storm times. *Journal of Geophysical Research*, *116*, A01203. https://doi.org/10.1029/2010JA015683

Yang, B., Zong, Q. G., Fu, S. Y., Takahashi, K., Li, X., Wang, Y. F., et al. (2011). Pitch angle evolutions of oxygen ions driven by storm time ULF poloidal standing waves. *Journal of Geophysical Research*, *116*, A03207. https://doi.org/10.1029/2010JA016047

Yang, B., Zong, Q.-G., Wang, Y. F., Fu, S. Y., Song, P., Fu, H. S., et al. (2010). Cluster observations of simultaneous resonant interactions of ULF waves with energetic electrons and thermal ion species in the inner magnetosphere. *Journal of Geophysical Research*, *115*, A02214. https://doi.org/10.1029/2009JA014542

Yokota, S., Kasahara, S., Mitani, T., Asamura, K., Hirahara, M., Takashima, T., et al. (2017). Medium-energy particle experiments–ion mass analyzer (MEP-i) onboard ERG (Arase). *Earth, Planets and Space*, *69*(1), 172. https://doi.org/10.1186/s40623-017-0754-8

Zong, Q.-G., Wang, Y. F., Zhang, H., Fu, S. Y., Zhang, H., Wang, C. R., et al. (2012). Fast acceleration of inner magnetospheric hydrogen and oxygen ions by shock induced ULF waves. *Journal of Geophysical Research*, *117*, A11206. https://doi.org/10.1029/2012JA018024